SCEC project #14061**: Prediction uncertainty in kinematic source modeling (PI: J.-P. Ampuero, Caltech)**

Project Abstract

We recently developed a general approach to explicitly handle Earth model inadequacies when computing geodetic predictions (forward models) in earthquake source inversion problems. We extended this new formalism to seismic predictions. Using this new approach, we can move from traditional deterministic approaches to more appropriate stochastic forward modeling approaches, enabling more rigorous quantification of uncertainties in fault slip inverse problems. In addition, prediction uncertainty dictates the relative weighting between geodetic, tsunami and seismic dataset for a given earthquake source problem. These advances lay the groundwork for a new generation of kinematic source models based on a general formalism that rigorously quantifies and incorporates the impact of uncertainties in fault slip inverse problems.

We applied this new formalism to actual observations in two cases using a Bayesian sampling approach: (1) the study of fault coupling along the San Andreas Fault and (2) the recent 2014 Mw=8.1 Pisagua earthquake. In these two cases, we derived the slip posterior probability density function using a Bayesian approach, including a full description of the data covariance and accounting for uncertainty in the elastic structure of the crust.

Exemplary figure

Figure 3: From Duputel et al. (in prep). Probabilistic slip model of the April 1st, 2015 Mw 8.1 Pisagua earthquake inferred from InSAR, GPS, tsunami and strong motion data, accounting for uncertainty in the Earth model. Arrows and their associated 95% error ellipses indicate the slip direction and uncertainty. Red star is the inverted hypocenter location. Gray lines are a posterior set of 1000 rupture fronts shown every 10 sec. Bottom left inset shows the posterior ensemble of moment rate functions.

SCEC project #14061: Prediction uncertainty in kinematic source modeling (PI: J.-P. Ampuero, Caltech)

1. Summary

With the bounty of modern data, we can develop new constraints on the behavior of faults, enabling us to study the distribution of slip during and after an earthquake and understand the seismo-tectonics of the surrounding region. Despite the ever-increasing number of geophysical observations available in the age of big data, a significant challenge in earthquake source inversions arises from *prediction errors*, i.e. imperfect predictions of the seismic wavefield due to uncertainties in Earth structure - the impact of which is generally overlooked. Indeed, for large earthquakes our ability to measure ground motions far exceeds our ability to model them.

We recently developed a general formalism to explicitly handle inadequacies of our predictions in static source inversions. More precisely, we built a physically based stochastic forward model to treat the model prediction uncertainty and show how it can be constructed to explicitly account for inaccuracies in the Earth model. Based on a first-order perturbation approach, our formalism relates prediction errors to uncertainties on the elastic parameters of different regions (e.g. crust, mantle, etc.). Such physical basis for our estimates of prediction uncertainty is expected to lead to more reliable images of the earthquake rupture process.

We extended the suite of tools developed previously for static slip inversion problem to the kinematic case. The most general problem being computationally challenging for the kinematic problem, we assume uncertainties in the depth-distribution of elastic parameters. Our synthetic scenarios exemplified that our realistic stochastic predictions produce more reliable source models that are resistant to over-fitting of data and includes realistic estimates of uncertainty on inferred model parameters.

We applied these tools to actual observations in two cases:

1. We used high-resolution SAR- and GPS-derived observations of surface displacements to derive the first probabilistic estimates of fault coupling along the creeping section of the San Andreas Fault (Jolivet et al., 2015). The inferred locked asperities are consistent with evidence for earthquakes of magnitude M > 6 over the past century in this area, and may be associated with the initiation phase of the 1857 M_w = 7.9 Fort Tejon earthquake. As creeping segments may be related to the initiation and termination of seismic ruptures, such distribution of locked and creeping asperities highlights the central role of the creeping section on the occurrence of major earthquakes along the San Andreas Fault.

2. We analyzed the recent 2014 Mw=8.1 Pisagua earthquake. We combined a wide range of observations including GPS, InSAR, tsunami and seismic data in order to obtain the most reliable kinematic slip model to date (Duputel et al., in prep). Our results shown in Fig. 1 indicate a very localized rupture with large slip, releasing the accumulated slip deficit in a small portion of the north Chilean seismic gap. Our model also shows that this earthquake did not rupture up to the trench. Assuming uniform coupling in the unbroken portion of the subduction zone, this leaves the possibility of occurrence of a major event driving slip at shallow depth, in a scenario similar to what was observed in Japan during the 2011 Tohoku-oki earthquake.

2. Technical report

2.1. Implementation of Cp for kinematic source inversion problems

With support from SCEC, we have recently developed a new formalism allowing us to account for prediction uncertainties (Duputel et al., 2014). Our formalism is based on a perturbation approach, assuming that the actual displacement field can be modeled as a perturbation of our predictions:

$$\begin{aligned}\mathbf{p}(\mathbf{E}_{\text{true}}, \mathbf{m}) &= \mathbf{p}(\mathbf{E}_{\text{model}} + \boldsymbol{\delta}\mathbf{E}, \mathbf{m}) \\ &\approx \mathbf{p}(\mathbf{E}_{\text{model}}, \mathbf{m}) + \frac{\partial \mathbf{p}}{\partial E_j}(\mathbf{E}_{\text{model}}, \mathbf{m}) \cdot \delta E_j + O(\boldsymbol{\delta}\mathbf{E}^2),\end{aligned}$$

where $\mathbf{p}(\mathbf{E}, \mathbf{m})$ is the predicted displacement field for the source model $\mathbf{m}$ based on Earth model $\mathbf{E}$ and $\mathbf{E}_{\text{model}}$ is the set of parameters used to approximate the "true" Earth $\mathbf{E}_{\text{true}}$ (i.e., density and elastic parameters). Under this assumption, if $\boldsymbol{C}_E$ represents the a priori covariance describing the uncertainty on the Earth model parameters $\mathbf{E}$, we can write the prediction error covariance as

$$\mathbf{C}_p = \mathbf{K} \cdot \boldsymbol{C}_E \cdot \mathbf{K}^T,$$

$$\text{where } K_{ij}(\mathbf{E}_{\text{model}}, \mathbf{m}) = \frac{\partial p_i}{\partial E_j}(\mathbf{E}_{\text{model}}, \mathbf{m}).$$

The covariance matrix $\mathbf{C}_p$ describes uncertainty, spatial and temporal correlations of the predicted waveforms. In the equation above, $\mathbf{K}$ can be interpreted as the full sensitivity matrix, i.e., the sensitivity of our predictions to perturbations in the elastic structure.

Calculation of $\mathbf{K}$ in the kinematic case is computationally challenging. There are various ways to estimate the sensitivity of predictions to perturbations in the Earth model. Most source inversions are based on layered Earth models, for which the computational load is reduced. Moreover, we are not interested in assigning uncertainties on a fine mesh but rather in describing uncertainties in a limited number N_E of tectonically defined regions (e.g., crust, mantle, etc).

The two left columns in Table 1 present a comparison of the computational load for a single evaluation of $\mathbf{C}_p$ using different strategies for the calculation of $\mathbf{K}$. One can use the Born approximation and take advantage of the Green tensor reciprocity to adopt an adjoint formulation (cf., "Adjoint" in Table 1). This approach is popular today in seismic tomography (Tromp et al. 2005) and can be used to calculate waveform sensitivity to 3D heterogeneities assuming a layered reference model. If we are only interested in the sensitivity to 1D heterogeneities, the most efficient approach is to use a conventional finite-difference approximation of the Fréchet derivatives in $\mathbf{K}$ (cf., "FD" in Table 1). Using forward finite-differences, this approach only requires 1 reference simulation and 3 simulations per perturbed layer (for V_p, V_s and ρ). Uncertainty on layer thicknesses can also be accounted for by performing one additional simulation per perturbed interface.

We implemented the calculation of $\mathbf{C}_p$ for the kinematic case in ALTAR, a transitional fully Bayesian sampling algorithm allowing to address very high-dimensional inverse problems. This implementation is based on GPU and currently enables the calculation of $\mathbf{C}_p$ for static and kinematic slip inversion problems assuming a tabular reference Earth model. A possible integration with SPECFEM3D to consider 3D perturbations will also be explored in the future. Another challenge is the dependence of $\mathbf{C}_p$ upon the source model $\mathbf{m}$. In the current implementation, we recognize that the prediction uncertainty must depend on the solution of the inverse problem by updating $\mathbf{C}_p$ at each transitional stage in ALTAR (Duputel et al., 2014).

	On the fly calculation of $\mathbf{K}$ for a single evaluation of $\mathbf{C}_p$		Pre-calculation of $\mathbf{K}^G$ for each Green's functions	
Simulation type	Adjoint - $\mathbf{K}$ 3D perturbations	FD - $\mathbf{K}$ 1D perturbations	Adjoint - $\mathbf{K}^G$ 3D perturbations	FD - $\mathbf{K}^G$ 1D perturbations
Number of simulations	$N_s + 1$	$3 \cdot N_E + 1$	$2 \cdot N_p \cdot (N_s + 1)$	$6 \cdot N_p \cdot N_E + 2 \cdot N_p$
Memory requirements	$12 \cdot N_D \cdot N_E$	$12 \cdot N_D \cdot N_E$	$24 \cdot N_p \cdot N_D \cdot N_E$	$24 \cdot N_p \cdot N_D \cdot N_E$
Example for $N_E = 8$, $N_p = 200$, $N_s = 100$, $N_D = 30000$				
Number of simulations	101 simul.	25 simul.	40400 simul.	10000 simul.
Memory requirements	2.9 MB	2.9 MB	1.2 GB	1.2 GB
Comp. Time on 400CPUs	4 min	1 min	23 hours	6 hours

Table 1. Computational load using different strategies for the calculation of sensitivity kernels in a 1D reference Earth model. The two first columns present the computational resources required for a single evaluation of C_p and the two last columns are for pre-computed sensitivity kernel for each Green's function. Adjoint calculation (for 3D perturbations) as well as forward finite-difference estimation of Fréchet derivatives (FD, for 1D perturbations) are considered. The Earth model is discretized in N_E regions with uniform uncertainty on V_p, V_s and ρ. We assume a dataset of N_s channels, a total of N_D data points and N_p fault patches. An example is provided assuming N_p=200, N_s=100, N_D=30000 and N_E=8. The computation time on 400 CPUs estimated using the discrete wavenumber method (Bouchon, 1977) at regional distance is provided.

2.2. Aseismic slip and seismogenic coupling along the central San Andreas Fault

Modern space geodetic techniques enable explorations of the kinematics of active faults during the inter-, co- and post-seismic phases of the earthquake cycle. Such exploration leads to the identification of regions where faults are locked, or coupled, accumulating elastic strain that can drive future earthquakes, and those where faults are slipping aseismically during the inter- and post-seismic periods (e.g. Thatcher , 1979). Using the tools developed previously to compute $\mathbf{C}_p$ in static source inversion problems (Duputel et al., 2014), we used high-resolution SAR- and GPS-derived observations of surface displacements to derive the first probabilistic estimates of fault coupling along the creeping section of the San Andreas Fault (Jolivet et al., 2015). We assume uncertainties in the depth-distribution of the shear modulus based on a three-dimensional seismic velocity model constructed from both absolute and differential times (Lin et al., 2010).

We represent in Figure 4 the posterior mean model and the cumulative PDF of fault coupling on different regions of the fault (i.e., the curves indicate the probability that fault coupling is lower than the value along the x-axis). We infer a high probability for significant elastic strain build up (~1 cm/yr) along the fast creeping section. In addition, we find a high probability of significant coupling on several asperities on the edges of the creeping segment, including the well-known Parkfield asperity and two newly inferred asperities to the north. We suggest that these asperities may correspond to the foreshocks of the 1857 M7.9 Fort Tejon earthquake. The significant strain build up along the creeping section, the presence of transition zones with locked asperities on the edges of the fastest creeping region and the possible implication of creep in the initiation of the 1857 earthquake underscore the importance of the creeping segment on the past and future seismic behavior of the San Andreas Fault.

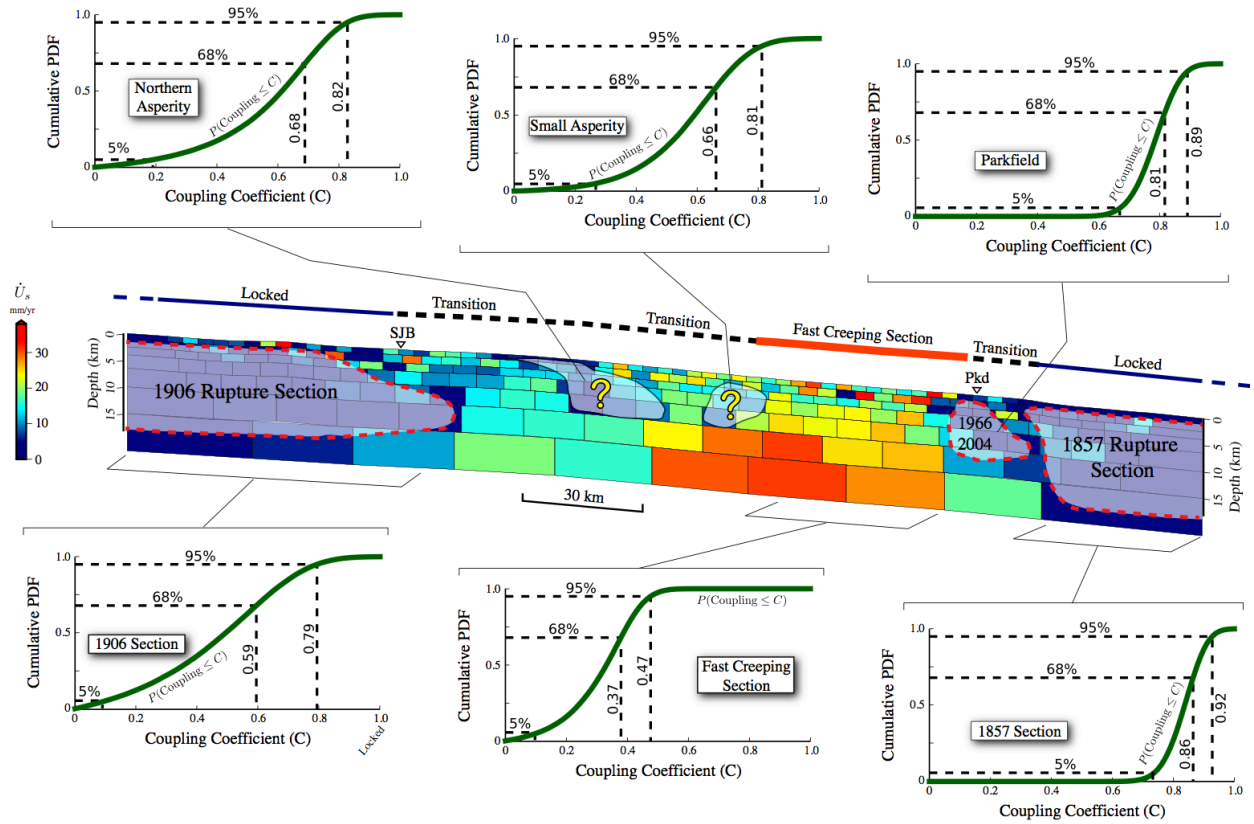

Figure 1. From Jolivet et al. (2015). Seismic and aseismic asperities along the central San Andreas fault - Color represents the mode of the a posteriori PDF of slip in the along-strike direction. Semi-transparent areas marked with red dashed lines correspond to asperities where significant earthquakes are known to have occurred, including the 1857 M7.9 Fort Tejon, 1906 M7.9 San Francisco and 1966 and 2004 M6.0 Parkfield earthquakes. White transparent areas with question marks are zones that are inferred to be coupled and the potential source for future earthquakes.

2.3. The Mw=8.1 Pisagua Earthquake of 1 April 2014

On 1 April 2014, northern Chile experienced a great earthquake that ruptured the central portion of the North Chile seismic gap. This event was preceded by two weeks of intense foreshock activity and followed by a large Mw=7.7 aftershock. Several co-seismic slip models have been proposed for the mainshock (An et al., 2014; Lay et al., 2014; Ruiz et al., 2014; Schurr et al., 2014; Yagi et al., 2014). These models show similar first-order features but also significant differences such as the extent, location and updip limit of the primary slip zone. Using the static and kinematic implementation of $\mathbf{C}_p$ detailed in 2.1, we combined a wide range of observations (InSAR, GPS, tsunami, high-rate GPS and strong motion data) in order to obtain the most reliable co-seismic slip model to date for this earthquake (Duputel et al., in prep). Our goal is not only to obtain a trustworthy slip distribution but also to produce realistic posterior uncertainty estimates, which can impact our interpretation of the rupture process.

Our approach is based on a meticulous error analysis accounting for uncertainty in P-wave velocity, S-wave velocity and density as a function of depth (Figure 2), while avoiding non-physical spatial smoothing over the slip distribution. In order to sample the high-dimensional model space of the joint static-kinematic source problem, we generated a large number of samples (i.e., more than 31 billion models, using 150,000 Markov chains).

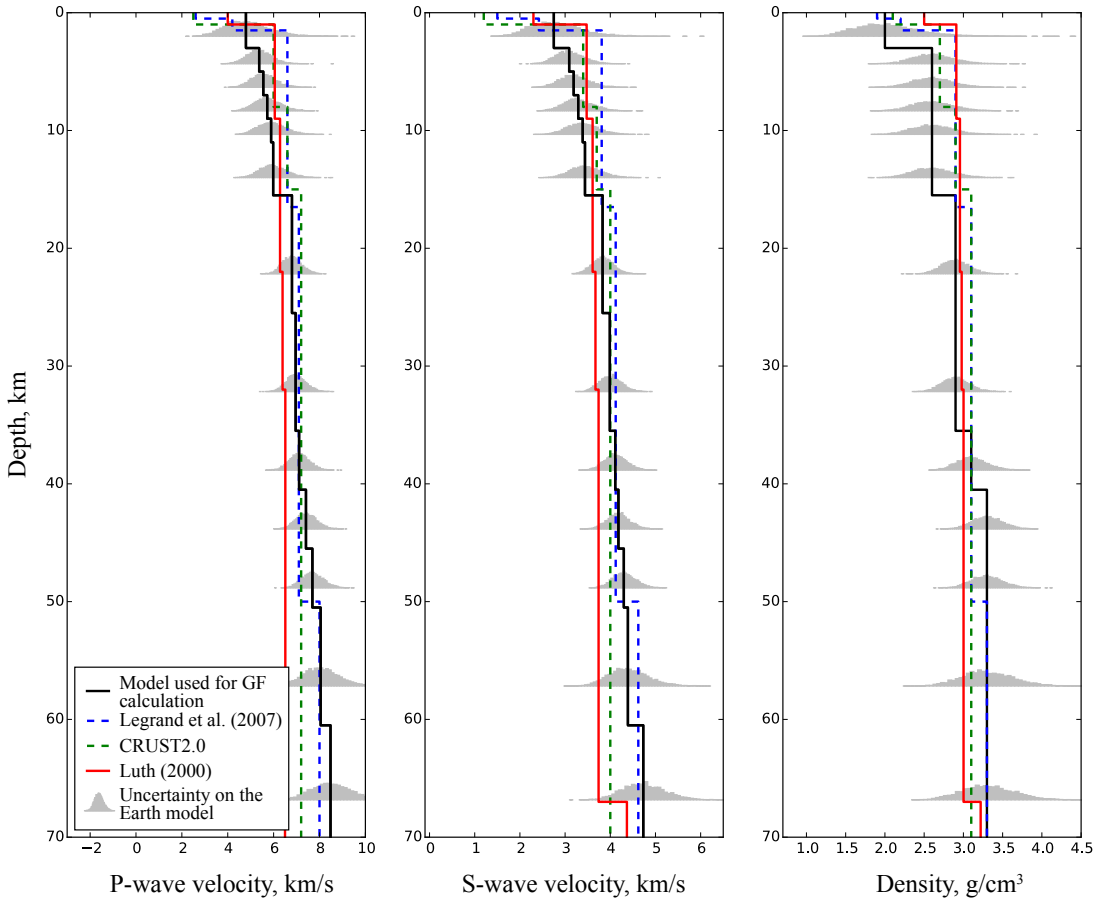

Figure 2: From Duputel et al. (in prep). Earth model uncertainty - (dashed green) P-wave velocity, S-wave velocity and Density from CRUST2.0, (dashed blue) from model E of Legrand et al. (2007), (red) from results of Luth (2000) and (black) minimum 1D model of Husen et al. [1999, used in this study for static and kinematic Green's function (GF) calculations]. Gray histograms are the probability density functions representing our confidence level on the elastic properties, as used to build the model prediction error. Histograms are derived from the 1D central model and the associated uncertainties, assuming a log-normal distribution (Duputel et al., 2014).

Figure 3 shows the posterior mean model and the associated uncertainty. We also present the posterior ensemble of moment rate functions in the bottom left inset of Figure 3. As reported previously, the Pisagua earthquake shows an unusual initiation phase with a very small moment rate in the first 20 sec. The southward rupture propagated initially with a relatively low average velocity (~1.8 km/s) and concentrated at the edge of a large slip patch that ruptured subsequently. This primary slip zone is more compact and involve larger slip than previously published results. This difference is probably due to the imposed spatial smoothing in previous slip models, which is absent in our Bayesian approach. Our model also shows that this earthquake did not rupture to the trench. It is not obvious if the shallow part of the North Chilean subduction is seismogenic or not (Metois et al., 2013) but if we assume uniform coupling in the unbroken portions of the seismic gap, failure in a single large event is certainly possible.

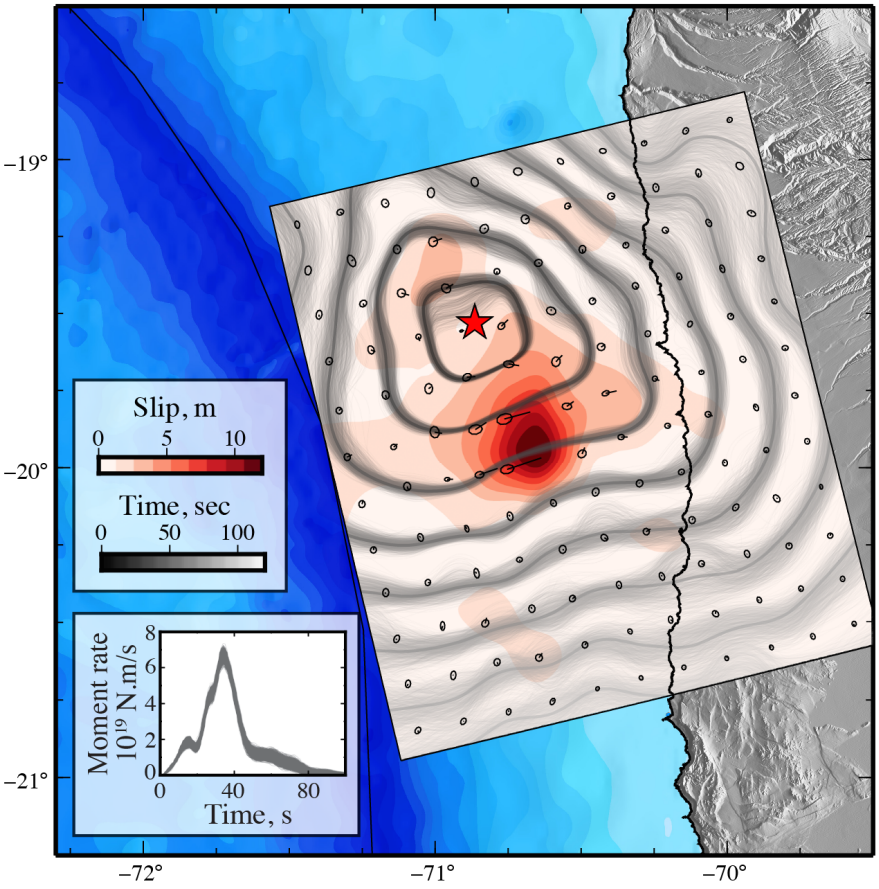

Figure 3: From Duputel et al. (in prep). Probabilistic slip model of the April 1st, 2015 Mw 8.1 Pisagua earthquake inferred from InSAR, GPS, tsunami and strong motion data, accounting for uncertainty in the Earth model. Red colors indicate slip amplitude. Arrows and their associated 95% error ellipses indicate the slip direction and uncertainty. Red star is the inverted hypocenter location. Gray lines are a posterior set of 1000 rupture fronts shown every 10 sec. Bottom left inset shows the posterior ensemble of moment rate functions.

3. Intellectual merit

Our research attempts to enable a new generation of kinematic earthquake source model that are more resistant to over-fitting of data, provide a physical basis for the relative weighting between disparate data sets, and include more realistic estimates of uncertainty on inferred model parameters. This effort exploits recent advances in Bayesian earthquake source modeling and new massively parallel computational approaches using GPUs. The benefits of this approach include improving the sharpness of our images of seismic and aseismic fault slip processes - thereby directly impacting both our models for fault mechanics and inferences of seismic hazard.

Our research addresses the following SCEC4 research priorities and requirements:

- 2a: The tools we developed support the "improvement of earthquake catalogs, including non-point-source source descriptions" by providing a general framework to have realistic error estimates on point-source and finite-fault model parameters.

- 3c: Our results support "theoretical and numerical modeling of specific fault resistance mechanisms for seismic radiation and rupture propagation", by assessing the reliability of seismological constraints on such processes.
- 6b: By providing better constraints on the earthquake rupture, our results contribute to "modeling of ruptures that includes realistic dynamic weakening mechanisms, off-fault plastic deformation, and is constrained by source inversions", and to "produce physically consistent rupture models for broadband ground motion simulation."

Our research directly addresses a priority for FARM: "propose source-inversion methods with minimal assumptions, and provide robust uncertainty quantification of inferred source parameters". It also relates to Computational Science disciplinary activities: "provide tools and algorithms for uncertainty quantification in large-scale inversion and forward-modeling studies", and Seismology disciplinary activities: "develop strategies for robust uncertainty quantification in finite-fault rupture models".

4. Broader impacts

This project provided training and research opportunities for a postdoctoral scholar, Zacharie Duputel, who is now hired as a CNRS researcher in France. He continues to lead this project, especially through regular visits to Caltech. The multidisciplinary research addressed herein gathered together geodesists, seismologists and computational scientists.

The algorithms and methods developed here are now directly applicable to other crustal deformation problems such as models of volcano deformation or to rapid source estimations problems for warning purposes. As we have done in the past, all of our developed tools will be documented and openly available to the geophysical community as open source. Open source software for 3D kinematic rupture was developed, incorporated in the spectral element code SPECFEM3D, distributed and maintained online through the Computational Infrastructure for Geophysics.

5. References

See also section "Publications and presentations related to this project".

An, C., I. Sepulveda, and P. L. F. Liu, 2014. Tsunami source and its validation of the 2014 Iquique, Chile, earthquake. Geophys. Res. Lett., 41(11), 3988–3994.

Duputel, Z., P. S. Agram, M. Simons, S. E. Minson, J. L. Beck, 2014. Accounting for prediction uncertainty when inferring subsurface fault slip. Geophys. J. Int., in press, doi: 10.1093/gji/ggt517 (SCEC contribution number 1791).

Duputel, Z., J. Jiang, R. Jolivet, M. Simons, L. Rivera, J.-P. Ampuero, B. Riel, S. E. Minson. The Mw=8.1 Pisagua Earthquake of 1 April 2014. In preparation for Geophys. Res. Lett.

Husen, S., E. Kissling, E. Flueh, and G. Asch, 1999. Accurate hypocentre determination in the seismogenic zone of the subducting Nazca Plate in northern Chile using a combined on-/offshore network. Geophys. J. Int., 138(3), 687–701, doi:10.1046/j.1365-246x.1999.00893.x.

Jolivet, R., Simons, M., Agram, P. S., Duputel Z., Shen, Z.-K., 2015. Aseismic slip and seismogenic coupling along the central San Andreas Fault, Geophysical Research Letters, v. 42, pp. 1-10

Lay, T., H. Yue, E. E. Brodsky, and C. An, 2014. The 1 April 2014 Iquique, Chile, Mw 8.1 earthquake rupture sequence. Geophys. Res. Lett., 41(11), 3818–3825.

Legrand, D., B. Delouis, L. Dorbath, C. David, J. Campos, L. Marquéz, J. Thompson, and D. Comte, 2007. Source parameters of the Mw=6.3 Aroma crustal earthquake of July 24, 2001 (northern Chile), and its aftershock sequence, Journal of South American Earth Sciences, 24(1), 58–68.

Lin, G., C. H. Thurber, H. Zhang, E. Hauksson, P. M. Shearer, F. Waldhauser, T. M. Brocher, and J. Hardebeck, 2010. A California Statewide Three-Dimensional Seismic Velocity Model from Both Absolute and Differential Times. Bull. Seismol. Soc. Am., 100(1), 225–240, doi: 10.1785/0120090028.

Lüth, S., 2000. Results of wide-angle investigations and crustal structure along a traverse across the central andes at 21 degrees south, Berliner Geowissenschaftliche Abhandlungen, Institute of Geology, Geophysics and Geoinformatics, Free University of Berlin, Berlin.

Metois, M., A. Socquet, C. Vigny, D. Carrizo, S. Peyrat, A. Delorme, E. Maureira, M. C. Valderas-Bermejo, I. Ortega, 2013. Revisiting the North Chile seismic gap segmentation using GPS-derived interseismic coupling. Geophys. J. Int., 194(3), 1283–1294.

Minson, S. E., M. Simons, J. L. Beck, 2013. Bayesian inversion for finite fault earthquake source models I - Theory and algorithm. Geophys. J. Int., 194, 1701-1726.

Ruiz, S., M. Metois, A. Fuenzalida, J. Ruiz, F. Leyton, R. Grandin, C. Vigny, R. Madariaga, and J. Campos, 2014. Intense foreshocks and a slow slip event preceded the 2014 Iquique Mw 8.1 earthquake. Science, 345(6201), 1165–1169.

Ryder, I., and R. Bürgmann, 2008. Spatial variations in slip deficit on the central San 426 Andreas Fault from InSAR. Geophys. J. Int., 175 (3), 837–852.

Schurr, B., G. Asch, S. Hainzl, J. Bedford, A. Hoechner, M. Palo, R. Wang, M. Moreno, M. Bartsch, Y. Zhang, O. Oncken, F. Tilmann, T. Dahm, P. Victor, S. Barrien- tos, and J.-P. Vilotte, 2014. Gradual unlocking of plate boundary controlled initiation of the 2014 Iquique earth- quake. Nature, 512(7514), 299–302.

Tarantola, A., B. Valette, 1982. Inverse problems = quest for information. J. Geophys. 50, 159–170.

Tromp, J., C. Tape, Q. Liu, 2005. Seismic tomography, adjoint methods, time reversal and banana-doughnut kernels. Geophys. J. Int. 160, 195–216.

Yagi, Y., R. Okuwaki, B. Enescu, S. Hirano, Y. Yamagami, S. Endo, and T. Komoro, 2014. Rupture process of the 2014 Iquique Chile Earthquake in relation with the fore- shock activity. Geophys. Res. Lett., 41(12), 4201–4206.

6. Publications and presentations related to this project

Avouac, J.-P., Ayoub, F., Wei, S., Ampuero, J.-P., Meng, L., Leprince, S., Jolivet, R., Duputel, Z. and D. Helmberger, 2013, Seismic slip boosted on a misoriented fault bend during the 2013, Mw7.7 Balochistan Earthquake, Earth Planet. Sci. Lett., 391, 128–134.

Duputel, Z., Jiang, J., Jolivet, R., Simons, M., Rivera, L., Ampuero, J.-P., Riel, B., Minson., S.E.. The Mw=8.1 Pisagua Earthquake of 1 April 2014. In preparation for Geophys. Res. Lett.

Duputel, Z., Jiang, J., Jolivet, R., Simons, M., Rivera, L., Ampuero, J.-P., Riel, B., Minson., S.E., Fielding. E., Klotz, J., Moore, A., Owen, S., Socquet, A., 2015. The Mw=8.1 Pisagua Earthquake of 1 April 2014. Presented at the 2014 AGU fall meeting, San Francisco, CA.

Duputel, Z., Simons, M., Ampuero, J.-P., Agram, P. S., Minson, S. E., J. L. Beck, 2013a. Toward accounting for prediction uncertainty when inferring subsurface fault slip, Presented at the 2013 SCEC Source Inversion Validation Workshop, Palm Springs, CA.

Duputel, Z., Simons, M., Agram, P. S., Minson and J.-P. Ampuero, 2013b. Toward the next generation of earthquake source models by accounting for model prediction error, Abstract G32B-07, Presented at the 2013 AGU fall meeting, San Francisco, CA.

Duputel, Z., Agram, P. S., Simons, M., Minson, S. E., Beck, J. L. 2014. Accounting for prediction uncertainty when inferring subsurface fault slip. Geophys. J. Int., in press, doi: 10.1093/gji/ggt517 (SCEC contribution number 1791).

Jolivet, R., Duputel, Z., Riel, B., Simons, M., Rivera, L., Minson, S. E., Zhang, H., Aivazis, M., Ayoub, F., Leprince, S., Avouac, J.-P., Samsonov, S., Motagh, M., Fielding, E., 2014. A fully Bayesian analysis of the 2013 Balochistan earthquake using long period seismic and space-based geodetic observations, Session S22C, Presented at the 2013 AGU fall meeting, San Francisco, CA.

Jolivet, R., Duputel, Z., Riel, B., Simons, M., Rivera, L., Minson, S. E., Zhang, H., Aivazis, M., Ayoub, F., Leprince, S., Avouac, J.-P., Samsonov, S., Motagh, M., Fielding, E., 2013. The 2013, Mw 7.7 Balochistan earthquake: Seismic potential of an accretionary wedge. Bull. Seism. Soc. Am., in press (SCEC contribution number 1899).

Jolivet, R., Simons, M., Agram, P. S., Duputel Z., Shen, Z.-K., 2015. Aseismic slip and seismogenic coupling along the central San Andreas Fault, Geophysical Research Letters, v. 42, pp. 1-10

Somala, S. N., J.-P. Ampuero and N. Lapusta, 2012, Earthquake source inversion with dense networks, Abstract S22A-07, presented at the 2012 AGU Fall Meeting, San Francisco, CA.

Somala, S.N., Ampuero, J.-P., and N. Lapusta, 2013a. Finite-fault source inversion using adjoint methods in 3D heterogeneous media, submitted to Geophys. J. Int.

S. N. Somala, J.-P. Ampuero and N. Lapusta (2014) Resolution of rise time in earthquake slip inversions: Effect of station spacing and rupture velocity Bull. Seismo. Soc. Am., 104 (6), 2717-2734, doi:10.1785/0120130185